



## Peristaltic Flow of the Bingham Plastic Fluid in a Curved Channel

Farah Alaa Adnan

[farrah.a\\_adnan@yahoo.com](mailto:farrah.a_adnan@yahoo.com)

Ahmad M. Abdul Hadi

Department of Mathematics, College of Science, University of Baghdad,  
Baghdad, Iraq.

Article history: Received 3 April 2019, Accepted 8 May 2019, Publish September  
2019

Doi:10.30526/32.3.2291

### Abstract

In this paper, we study the peristaltic transport of incompressible Bingham plastic fluid in a curved channel. The formulation of the problem is presented through, the regular perturbation technique for small values of  $\frac{1}{k}$  is used to find the final expression of stream function. The numerical solution of pressure rise per wave length is obtained through numerical integration because its analytical solution is impossible. Also the trapping phenomenon is analyzed. The effect of the variation of the physical parameters of the problem are discussed and illustrated graphically.

**Key words:** Bingham plastic fluid, a curved channel, Peristaltic transport, regular perturbation method.

### 1. Introduction

The peristaltic flows have a fundamental function in physiology and engineering. Many authors have investigated such flows like Adnan et al. studied the effect of the magnetic field on a peristaltic flow of Bingham plastic fluid [1]. Ahmed et al. investigated the effect of a magnetic field on peristaltic flow of Jeffery fluid through a porous medium in a tapered asymmetric channel [2]. Adnan et al. investigated the effect of a magnetic field on a peristaltic transport of Bingham plastic fluid in a symmetrical channel [3]. And Ahmad et al. studied the peristaltic transport of MHD flow and heat transfer in a tapered asymmetric channel through porous medium and the effect of variable viscosity, velocity – non slip and temperature jump are discussed [4]. The flows over the curved walls are considering as engineering advantage and happened for example in turbo machinery and the wings of airplane. And that's why it is fundamental to know the effect of curvature (which denoted by  $k$ ) on the channels. The peristaltic motion in curved channel is an important area of research because the shape of the most of the physiological tubes and glandular channels is curved. It have been seen from the available studies

that not a lot of attention is considering in the peristaltic flow in a curved channel. Ali et al. studied the peristaltic flow of a non-Newtonian fluid in a curved channel [5]. Hayat et al. studied the peristaltic transport of viscous fluid with compliant walls in curved channel [6]. Ahmad studied the effect of radial magnetic field on peristaltic transport of Jeffrey fluid with variable viscosity in curved channel with heat and mass transfer properties [7]. Kalantari et al. investigated the effect of radially imposed magnetic field on the flow characteristics in a curved channel [8]. Norenn et al. studied the curvature effects on the MHD peristaltic flow of an incompressible Carreau fluid in a curved channel [9]. Hina et al. studied the slip conditions effect on the peristaltic transport of Johnson-Segalman fluid through a curved channel [10-12]. In this paper, the peristaltic transport of Bingham plastic fluid in a curved channel has been discussed. The concept of large wave length  $\lambda$  and small Ronald's  $Re$  is used to simplify the equation. The nonlinear differential equation is solved analytically by the regular perturbation method for small values of  $\frac{1}{k}$  where  $k$  is the curvature of the channel. The impact of the different physical parameters on the velocity axial, the local shear stress, the pressure gradient, pressure rise and trapping phenomenon are discussed in detail with the use of the graphs.

## 2. Problem Statement

Assume the peristaltic flow of an incompressible Bingham plastic fluid in a curved channel of thickness  $2a$  convolute in a circle with center  $O$  and radius  $R^*$  where the space inside the channel is filled with Bingham plastic fluid. The velocity components in radial  $\bar{R}$  and axial  $\bar{X}$  direction are  $\bar{V}$  and  $\bar{U}$  respectively. The flow of Bingham plastic fluid in the curved channel consequent to the contraction and dilation of the flexible walls of the channel where the inertial force effects are taken small. The walls of the channel are described mathematically as follows:

$$\begin{aligned} \bar{H}(\bar{X}, \bar{t}) &= a + b \sin \left[ \frac{2\pi}{\lambda} (\bar{X} - c\bar{t}) \right], & \text{Upper wall} \\ -\bar{H}(\bar{X}, \bar{t}) &= -a - b \sin \left[ \frac{2\pi}{\lambda} (\bar{X} - c\bar{t}) \right], & \text{Lower wall} \end{aligned} \quad (1)$$

Where  $c$  is the speed,  $b$  is the amplitude of wave along the upper and lower walls and  $\lambda$  is the wave length. The wave length is taken large however in more realistic situations it depends on time as the contraction and dilation in natural systems are account on varying  $\lambda$ . The width of curved channel perpendicular to the plane is supposed to be infinite so the flow can safely be taken as two dimensional. The flow is assumed to be laminar. Then the velocity field which is consider as the following form:

$$\bar{V} = [\bar{V}(\bar{R}, \bar{X}, \bar{t}), \bar{U}(\bar{R}, \bar{X}, \bar{t}), 0]$$

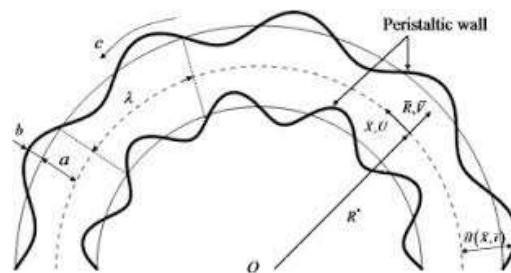


Figure 1. The geometry of the curved channel.

For an incompressible Bingham plastic fluid the conservation of mass and momentum for the velocity field are given as follows:

$$\nabla \cdot \bar{V} = 0$$

$$\rho \left( \frac{\partial \bar{V}}{\partial t} + (\bar{V} \cdot \nabla) \bar{V} \right) = -\nabla \bar{P} + \nabla \cdot \bar{\tau} \tag{2}$$

Where  $\rho$  is the density of the fluid,  $\bar{P}$  is the pressure and  $\bar{\tau}$  is the stress tensor.

$$\frac{\partial \bar{V}}{\partial \bar{R}} + \frac{R^*}{R^* + \bar{R}} \frac{\partial \bar{U}}{\partial \bar{X}} + \frac{\bar{V}}{R^* + \bar{R}} = 0 \tag{3}$$

$$\rho \left[ \frac{\partial \bar{V}}{\partial \bar{t}} + \bar{V} \frac{\partial \bar{V}}{\partial \bar{R}} + \frac{R^* \bar{U}}{R^* + \bar{R}} \frac{\partial \bar{V}}{\partial \bar{X}} - \frac{\bar{U}^2}{R^* + \bar{R}} \right] = -\frac{\partial \bar{P}}{\partial \bar{R}} + \frac{1}{R^* + \bar{R}} \frac{\partial}{\partial \bar{R}} [(R^* + \bar{R}) \bar{\tau}_{\bar{R}\bar{R}}] + \left( \frac{R^*}{R^* + \bar{R}} \right) \frac{\partial \bar{\tau}_{\bar{R}\bar{X}}}{\partial \bar{X}} - \frac{\bar{\tau}_{\bar{X}\bar{X}}}{R^* + \bar{R}} \tag{4}$$

$$\rho \left[ \frac{\partial \bar{U}}{\partial \bar{t}} + \bar{V} \frac{\partial \bar{U}}{\partial \bar{R}} + \frac{R^* \bar{U}}{R^* + \bar{R}} \frac{\partial \bar{U}}{\partial \bar{X}} + \frac{\bar{U} \bar{V}}{R^* + \bar{R}} \right] = -\left( \frac{R^*}{R^* + \bar{R}} \right) \frac{\partial \bar{P}}{\partial \bar{X}} + \frac{1}{(R^* + \bar{R})^2} \frac{\partial}{\partial \bar{R}} [(R^* + \bar{R})^2 \bar{\tau}_{\bar{R}\bar{X}}] + \left( \frac{R^*}{R^* + \bar{R}} \right) \frac{\partial \bar{\tau}_{\bar{X}\bar{X}}}{\partial \bar{X}} \tag{5}$$

With the boundary conditions are taken in the forms as follows:

$$\bar{U} = 0 \text{ at } \mp \bar{H}(\bar{X}, \bar{t}) = \mp [a + b \sin \left[ \frac{2\pi}{\lambda} (\bar{X} - c\bar{t}) \right]] \tag{6}$$

In the Fixed frame of reference  $(\bar{R}, \bar{X})$ , the flow in the channel is unsteady. However it can be considered as steady in the wave frame with coordinate  $(\bar{r}, \bar{x})$  moving with speed  $c$ . the transformation equations that relating the two frames are given as follows:

$$\bar{x} = \bar{X} - c\bar{t}, \bar{r} = \bar{R}, \bar{u} = \bar{U} - c, \bar{v} = \bar{V}, \bar{P} = \bar{p} \tag{7}$$

and presenting the dimensionless quantities that used to find out the non-dimensional analysis as follows:

$$x = \frac{2\pi \bar{x}}{\lambda}, \eta = \frac{\bar{r}}{a}, u = \frac{\bar{u}}{c}, v = \frac{\bar{v}}{c}, p = \frac{2\pi a^2}{\lambda \mu c} \bar{p}, h = \frac{\bar{H}}{a}, \tau = \frac{a \bar{\tau}}{\mu c}, Re = \frac{\rho c a}{\mu}, \delta = \frac{2\pi a}{\lambda}, k = \frac{R^*}{a}, \varphi = \frac{b}{a}, \dot{\gamma} = \frac{\rho a^2}{\mu_0} \bar{\dot{\gamma}} \tag{8}$$

In which  $(u, v)$  are the non-dimensional velocity components,  $p$  is the non-dimensional pressure,  $\tau$  is the non-dimensional stress tensor,  $Re$  is the Ronald's number,  $\delta$  is the wave length ratio (wave number),  $k$  is the curvature parameter and  $\varphi$  is the amplitude ratio.

Making use of the equation (7) and the above dimensionless quantities, the continuity and the motion equations will be reduced as follows:

$$(k + \eta) \frac{\partial v}{\partial \eta} + k \delta \frac{\partial u}{\partial x} + v = 0 \tag{9}$$

$$-\delta^2 Re \frac{\partial v}{\partial x} + Re \delta v \frac{\partial v}{\partial \eta} + Re \delta \frac{k(u+1)}{k+\eta} \frac{\partial v}{\partial x} - Re \delta \frac{(u+1)^2}{k+\eta} = -\frac{\partial p}{\partial \eta} + \frac{\delta}{k+\eta} \frac{\partial}{\partial \eta} [(k + \eta) \tau_{\eta\eta}] + \delta^2 \left( \frac{k}{k+\eta} \right) \frac{\partial \tau_{\eta x}}{\partial x} - \delta \frac{\tau_{xx}}{ak+a\eta} \tag{10}$$

$$-Re \delta \frac{k+\eta}{k} \frac{\partial u}{\partial x} + Re \frac{k+\eta}{k} v \frac{\partial u}{\partial \eta} + Re \delta (u + 1) \frac{\partial u}{\partial x} + Re \frac{(u+1)v}{k} = -\frac{\partial p}{\partial x} + \frac{1}{k} \frac{1}{k+\eta} \frac{\partial}{\partial \eta} [(k + \eta)^2 \tau_{\eta x}] + \delta \frac{\partial \tau_{xx}}{\partial x} \tag{11}$$

The boundary conditions in non-dimensional parameters,

$$u + 1 = 0, \mp [h] = \mp [1 + \varphi \sin x] \tag{12}$$

And the stream function [11].

$$u = -\frac{\partial \psi}{\partial \eta}, v = \delta \frac{k}{\eta+k} \frac{\partial \psi}{\partial x} \tag{13}$$

Applying equation (13) on the equation (12).The boundary conditions becomes

$$\frac{\partial \psi}{\partial \eta} = 1, \bar{\tau}[h] = \bar{\tau}[1 + \varphi \sin x] \tag{14}$$

The general solution of the governing equations seems to be hard in most cases, therefore the solution can be found under the assumption of small wave number  $\delta \ll 1$  and low Reynolds number approximation, thus the equations (10) and (11) can be written as follows:

$$\frac{\partial p}{\partial \eta} = 0 \tag{15}$$

$$\frac{\partial p}{\partial x} = \frac{1}{k} \frac{1}{k+\eta} \frac{\partial}{\partial \eta} [(k + \eta)^2 \tau_{\eta x}] \tag{16}$$

Deriving equation with respect to  $\eta$ , one obtain:

$$\frac{\partial}{\partial \eta} \left[ \frac{1}{k} \frac{1}{k+\eta} \frac{\partial}{\partial \eta} [(k + \eta)^2 \tau_{\eta x}] \right] = 0 \tag{17}$$

Noticing that the Cauchy stress tensor  $\sigma^*$  can be decomposed as follows:

$$\sigma^* = -\bar{P}I + \bar{\tau}$$

Where  $\bar{\tau}$  is the extra stress tensor and  $\bar{P}$  is the mechanical pressure. The Bingham stresses  $\bar{\tau}_{ij}$  are related to the strain rates  $\bar{A}_1$  through the constitutive equation:

$$\bar{\tau}_{ij} = (2\mu_0 + \frac{\tau_y}{\bar{\gamma}}) \bar{A}_1 \text{ for } \tau \geq \tau_y$$

$$\bar{\tau}_{ij} = 0 \text{ for } \tau < \tau_y.$$

Where  $\tau_y$  is the yield stress,  $\mu_0$  is the Bingham fluid viscosity,  $\bar{\gamma} = \left(\frac{1}{2} \text{trac} \bar{A}_1^2\right)^{\frac{1}{2}}$ , and the final

$$\tau_{\eta x} = 2 \left( -\frac{\partial^2 \psi}{\partial \eta^2} - \frac{1}{k+\eta} \left(1 - \frac{\partial \psi}{\partial \eta}\right) \right) + Bn \tag{18}$$

Where  $\frac{\rho a^2 \tau_y}{\mu_0^2 Re} = \frac{a \tau_y}{\mu_0 c} = Bn$  the Bingham number. Substituting the above equation (18) into equation (17) one obtain:

$$\frac{\partial^4 \psi}{\partial \eta^4} + \frac{2}{(k+\eta)} \frac{\partial^3 \psi}{\partial \eta^3} - \frac{1}{(k+\eta)^2} \frac{\partial^2 \psi}{\partial \eta^2} + \left(\frac{\partial \psi}{\partial \eta} - 1\right) \frac{1}{(k+\eta)^3} = 0 \tag{19}$$

Noticing that the dimensionless mean flows  $\Theta$  in the fixed frame and  $F$  in the wave frame as:

$$\Theta = \frac{Q^*}{ac}, F = \frac{q}{ac} \text{ one get:}$$

$$\Theta = F + 2$$

In which:

$$F = - \int_{-h}^h \frac{\partial \psi}{\partial \eta} d\eta = -(\psi(h) - \psi(-h))$$

Then:

$$\psi(h) - \psi(-h) = -F$$

$\psi(h) = -\frac{F}{2}$  At the upper wall and  $\psi(-h) = \frac{F}{2}$  at the lower wall. The dimensionless pressure rise over wave length is defined by:

$$\Delta p_\lambda = \int_0^{2\pi} \frac{dp}{dx} dx$$

### 3. Methods of Solution for the Problem

Using the perturbation for small values of  $\frac{1}{k}$  by expanding the flow quantities in a power series of  $\frac{1}{k}$  as follows:

$$\begin{aligned} \psi &= \psi_0 + \frac{1}{k}\psi_1 + \frac{1}{k^2}\psi_2 + \frac{1}{k^3}\psi_3 \\ \frac{1}{k+\eta} &= \frac{1}{k} - \frac{\eta}{k^2} + \frac{\eta^2}{k^3} \\ \frac{1}{(k+\eta)^2} &= \frac{1}{k^2} - \frac{2\eta}{k^3} + \frac{3\eta^2}{k^4} \\ \frac{1}{(k+\eta)^3} &= \frac{1}{k^3} - \frac{3\eta}{k^4} + \frac{6\eta^2}{k^5} \end{aligned} \quad (20)$$

Substituting the above equation (20) into the equation (19) and then comparing the coefficients of the same power of  $\frac{1}{k}$  up to the second order the following systems will be obtained:

#### 3.1 The Zeroth Order

$$\frac{\partial^4 \psi_0}{\partial \eta^4} = 0 \quad (21)$$

Along with its boundary conditions:

$$\psi_0 = -\frac{F}{2}, \quad \frac{\partial \psi_0}{\partial \eta} = 1 \quad \text{at the upper wall}$$

$$\psi_0 = \frac{F}{2}, \quad \frac{\partial \psi_0}{\partial \eta} = 1 \quad \text{at the lower wall} \quad (22)$$

#### 3.2 The First Order

$$\frac{\partial^4 \psi_1}{\partial \eta^4} + 2 \frac{\partial^3 \psi_0}{\partial \eta^3} = 0 \quad (23)$$

Along with its boundary conditions:

$$\psi_1 = 0, \quad \frac{\partial \psi_1}{\partial \eta} = 0 \quad \text{at the upper wall}$$

$$\psi_1 = 0, \quad \frac{\partial \psi_1}{\partial \eta} = 0 \quad \text{at the lower wall} \quad (24)$$

#### 3.3 The Second Order

$$\frac{\partial^4 \psi_2}{\partial \eta^4} + 2 \frac{\partial^3 \psi_1}{\partial \eta^3} - 2\eta \frac{\partial^3 \psi_0}{\partial \eta^3} - \frac{\partial^3 \psi_0}{\partial \eta^3} = 0 \quad (25)$$

Along with its boundary condition:

$$\psi_2 = 0, \quad \frac{\partial \psi_2}{\partial \eta} = 0 \quad \text{at the upper wall}$$

$$\psi_2 = 0, \quad \frac{\partial \psi_2}{\partial \eta} = 0 \quad \text{at the lower wall} \quad (26)$$

Solving the above systems of the zeroth, first and second order by mathematic program, the final calculation for the stream function would be as follows:

$$\begin{aligned} \psi &= \\ &a_1 + a_2\eta + a_3\eta^2 + a_4\eta^3 + \frac{a_5 + a_6\eta + a_7\eta^2 + a_8\eta^3 - \frac{a_4\eta^4}{2}}{k} + \frac{a_9 + a_{10}\eta + a_{11}\eta^2 + a_{11}\eta^3 + \frac{1}{12}((a_3 - 6a_8)\eta^4 + \frac{21a_4\eta^5}{5})}{k^2} \end{aligned} \quad (27)$$

And,

$$\begin{aligned}
 a_1 &= -\frac{Fh_1^3 - 3Fh_1^2h_2 - 2h_1^3h_2 - 3Fh_1h_2^2 + Fh_2^3 + 2h_1h_2^3}{2(-h_1+h_2)^3}, \\
 a_2 &= -\frac{-h_1^3 - 6Fh_1h_2 - 3h_1^2h_2 + 3h_1h_2^2 + h_2^3}{(h_1-h_2)^3}, \quad a_3 = -\frac{3(F+h_1-h_2)(h_1+h_2)}{(h_1-h_2)^3}, \\
 a_4 &= \frac{2(F+h_1-h_2)}{(h_1-h_2)^3}, \quad a_5 = -\frac{1}{2}a_4h_1^2h_2^2, \quad a_6 = a_4h_1^2h_2 + a_4h_1h_2^2, \\
 a_7 &= \frac{1}{2}(-a_4h_1^2 - 4a_4h_1h_2 - a_4h_2^2), \quad a_8 = a_4h_1 + a_4h_2, \\
 a_9 &= \frac{1}{60}(5a_3h_1^2h_2^2 - 30a_8h_1^2h_2^2 + 42a_4h_1^3h_2^2 + 42a_4h_1^2h_2^3), \\
 a_{10} &= -\frac{1}{60}h_1(10a_3h_1h_2 - 60a_8h_1h_2 + 84a_4h_1^2h_2 + 10a_3h_2^2 - 60a_8h_2^2 + 147a_4h_1h_2^2 + \\
 &84a_4h_2^3), \quad a_{11} = \frac{1}{60}(5a_3h_1^2 - 30a_8h_1^2 + 42a_4h_1^3 + 20a_3h_1h_2 - 120a_8h_1h_2 + \\
 &168a_4h_1^2h_2 + 5a_3h_2^2 - 30a_8h_2^2 + 168a_4h_1h_2^2 + 42a_4h_2^3), \quad a_{12} = \frac{1}{60}(-10a_3h_1 + \\
 &60a_8h_1 - 63a_4h_1^2 - 10a_3h_2 + 60a_8h_2 - 84a_4h_1h_2 - 63a_4h_2^2)
 \end{aligned}
 \tag{28}$$

#### 4. Results and Discussion

This section presented the graphical description of different parameters on the out coming of flow quantities. The variation of the axial velocity, local shear stress, the pressure gradient, the pressure rise and the stream lines are illustrated and analyzed graphically.

##### 4.1 The Axial Velocity

The outcome in terms of different parameters of the axial velocity  $u(\eta)$  have been plotted as a function of  $\eta$  at  $x = \frac{\pi}{2}$  the wider part of the channel. It is clear from the figures that the axial velocity attains parabolic in nature other than some points of reflection on velocity curves which opposite the situation from increase to decrease and vice versa including the following figures. **Figure 2.** Describes the mixed behavior of small values of the curvature of the channel on the axial velocity profile. It is clear that the axial velocity profile is not symmetric at the central line of the channel  $\eta = 0$ , and the maximal of the profile shift to the end of the channel. However in **Figure 3.** For large values of  $k$  the axial velocity profile becomes symmetric at the central line of the channel  $\eta = 0$ . It has been noted that the axial velocity stops and fixed for large values of  $k$ . **Figure 4.** Studied the effect of  $\phi$  on the axial velocity, the graph that an increase in  $\phi$  increase the axial velocity profile near the walls and decreases the velocity profile at the central part of the channel. It also shows that the axial velocity profile is not symmetric at the central line of the channel  $\eta = 0$  and the axial velocity profile attains its maximal at the beginning of the channel. **Figure 5.** Portrays that for ascending values of the flow rate the axial velocity profile increases in the central part of the channel and decreases at the wall of the channel.

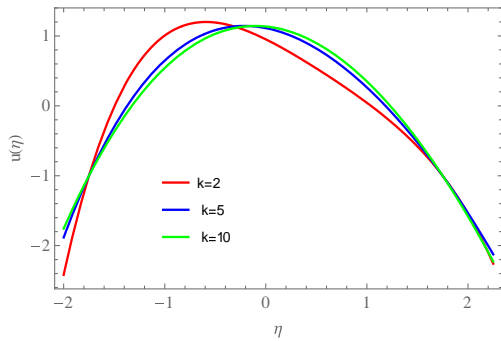


**Figure 2.**The velocity profile for fixed values of  $\phi = 0.75, F = 1.5$ .

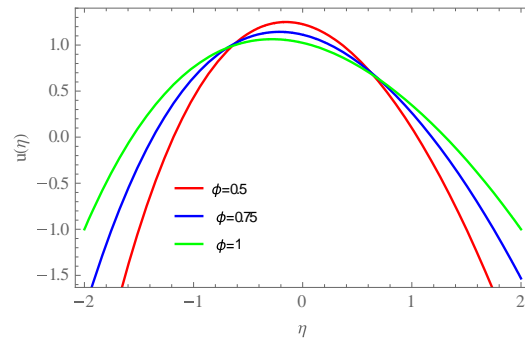


**Figure 4.**The velocity profile for fixed values of  $k = 5, F = 1.5$ .

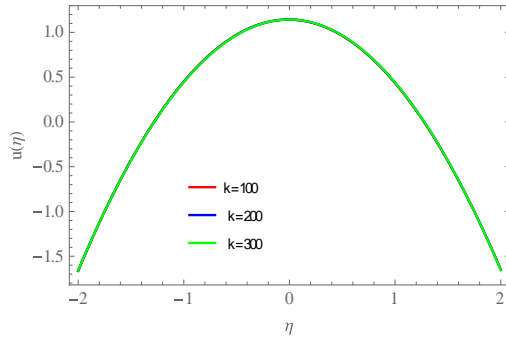


**Figure 3.**The velocity profile for fixed values of  $\phi = 0.75, F = 1.5$ .

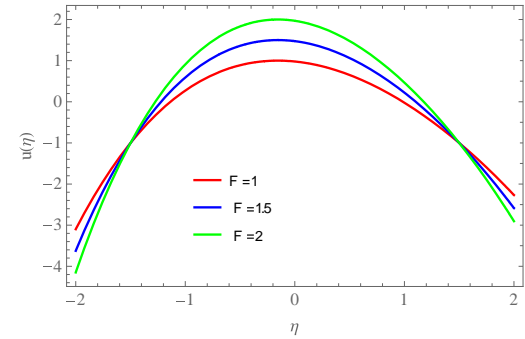


**Figure 5.**The velocity profile for fixed values of  $k = 5, \phi = 0.75$ .

#### 4.2 The Local Shear Stress

In this subsection, the discussions of the influence of the different parameters on the local shear stress were investigated. **Figure 6.** Discusses the variation of  $k$  on the magnitude of shear stress. It shows that the shear stress increases in the whole channel specially at the central part of the channel with an increase of  $k$ . However the shear stress stops increasing and fixed for large values of  $k$  as it is shown in **Figure 7.** **Figure 8.** Exhibits the effect of an increase of  $\phi$  on the shear stress. It is shown that when  $\phi$  increases the magnitude of shear stress decreases in ( $x < 0$  and  $x > 3$ ) and for  $0 \leq x \leq 3$  the magnitude of shear stress increases. **Figure 9.** Deduced that for large values of the flow rate  $F$  the shear stress is decreasing function in the whole channel. **Figure 10.** displays the impact of Bingham fluid number on the shear stress. It is noticed that the shear stress is an increasing function to the increase of Bingham fluid number  $Bn$ .

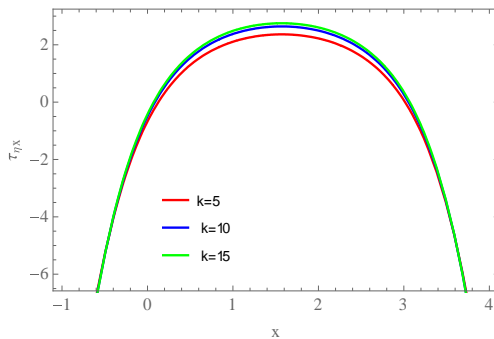


**Figure 6.** The shear stress for fixed values [ $\eta = 0.5, \phi = 0.5, F = 1.5, Bn = 5$ ].

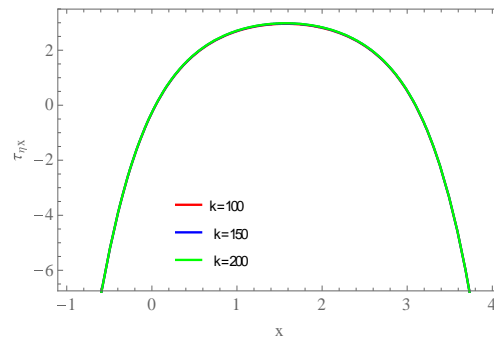


**Figure 7.** The shear stress for fixed values [ $\eta = 0.5, \phi = 0.5, F = 1.5, Bn = 5$ ].

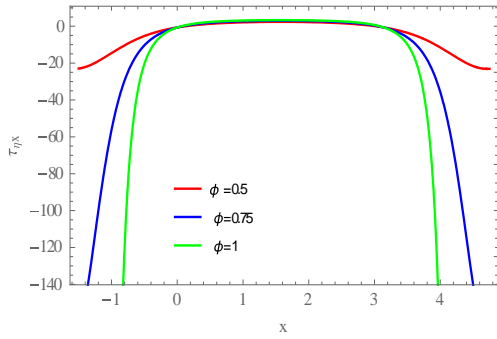


**Figure 8.** The shear stress for fixed values [ $\eta = 0.5, k = 5, F = 1.5, Bn = 5$ ].

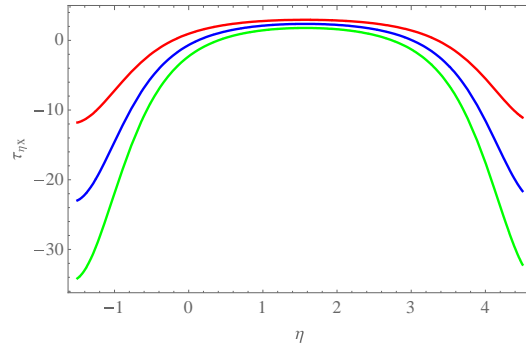


**Figure 9.** The shear stress for fixed values [ $\eta = 0.5, k = 5, \phi = 0.5, Bn = 5$ ].

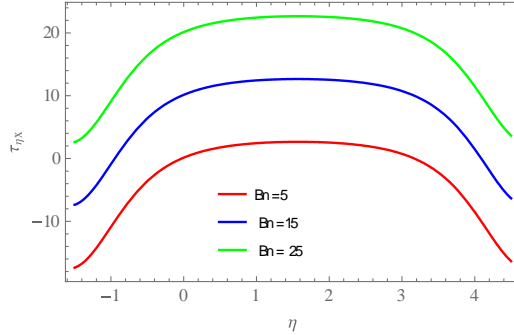


**Figure 10.** The shear stress for fixed values [ $\eta = 0.5, k = 5, \phi = 0.5, F = 1.5$ ].

### 4.3 The Pressure Gradient ( $\frac{dp}{dx}$ )

In this section the effect of the variation of different parameters on the pressure gradient is recorded in the following plots. **Figure 11.** Demonstrates that an increase in the value of  $k$  increases the pressure gradient curves. The interesting feature the pressure gradient stops increasing and fixed for large values of  $k$ . **Figure 12.** Portrays that for ascending values of flow rate the pressure gradient is decreasing function. **Figure 13.** Illustrates the effect of amplitude ratio parameter ( $\phi$ ) on the pressure gradient curves, when  $\phi$  increase the amounts of pressure gradient decreases at  $3 < x \leq 5$  and increase at the central part of the channel. **Figure 14.** Describes the effect of increasing the value of Bingham number  $Bn$  on the pressure gradient. It shows that The pressure gradient ( $\frac{dp}{dx}$ ) is decreasing function for the increase of  $Bn$ .

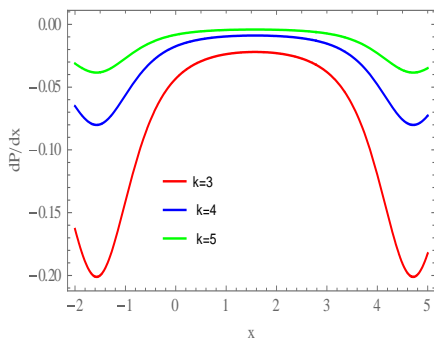


**Figure 11.** The pressure gradient for fixed values [ $\eta = 0.5, F = 1, \phi = 0.5, Bn = 5$ ].

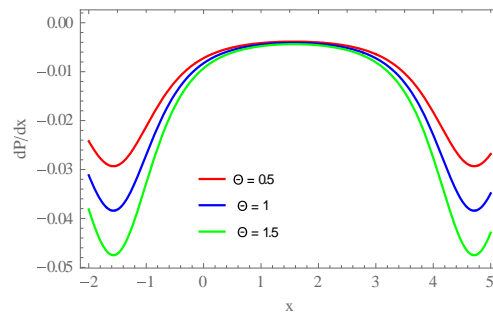


**Figure 12.** The pressure gradient for fixed values [ $\eta = 0.5, k = 5, \phi = 0.5, Bn = 5$ ].

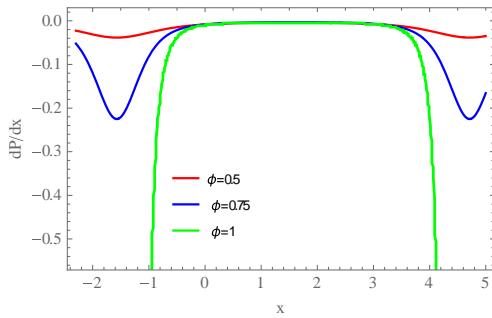


**Figure 13.**The pressure gradient for fixed values [ $\eta = 0.5, k = 5, F = 1, Bn = 5$ ].

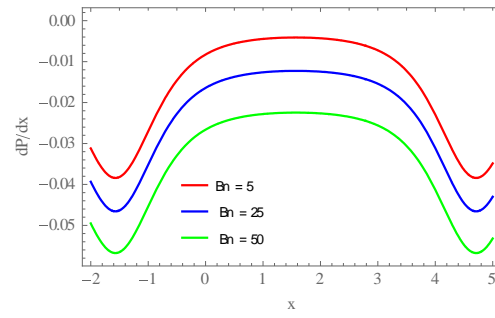


**Figure 14.**The pressure gradient for fixed values [ $\eta = 0.5, k = 5, F = 1, \phi = 0.5$ ].

#### 4.4 The Pressure Rise

The relationship between the non-dimensional average pressure rise per wave length and dimensionless mean flow rate  $\Theta$ . The following **Figurers 15-17**. Shows the variation of  $\Delta p$  against mean flow rate  $\Theta$  where a linear relationship between  $\Delta p$  and  $\Theta$  as it is shown in the figurers. The whole region is considered to five parts

1. Peristaltic pumping region where  $\Delta p > 0, \Theta > 0$ .
2. Augmented pumping (co- pumping region) where  $\Delta p < 0, \Theta > 0$  and no flow is recognize in this region.
3. Retrograde pumping region where  $\Delta p > 0, \Theta < 0$  and no flow is recognize in this region.
4. The co- pumping region where  $\Delta p < 0, \Theta < 0$ .
5. Free pumping region where  $\Delta p = 0$ .

**Figure 15**. discusses the variation of  $k$  on the pressure rise per wave length. It is observed that the pumping rate increases in the co- pumping region where  $\Delta p < 0, \Theta < 0$  while it is decreasing in the peristaltic pumping region where  $\Delta p > 0, \Theta > 0$ . **Figure 16**. Plots the effect of amplitude ratio parameter  $\phi$  on pressure rise per wave length, it has been noticed that an increase in  $\phi$  increase the pumping rate in the peristaltic pumping region( $\Delta p > 0, \Theta > 0$ ), and decrease the pumping rate in the co- pumping region ( $\Delta p < 0, \Theta < 0$ ). **Figure 17**. Shows the effect of an increase of Bingham number parameter  $Bn$  on the pressure rise per wave length, it shows that the pumping rate decreases in both peristaltic pumping region ( $\Delta p > 0, \Theta > 0$ ) and the co- pumping region( $\Delta p < 0, \Theta < 0$ ).

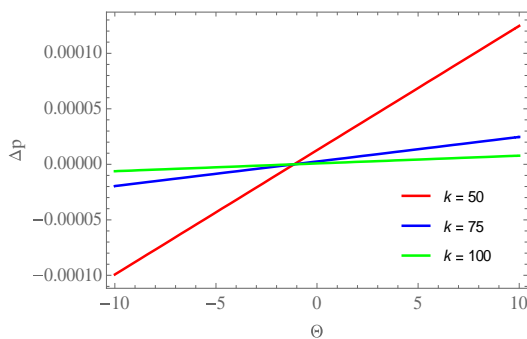


**Figure 15.** The pressure rise for fixed values [ $\phi = 0.5, Bn = 5$ ].

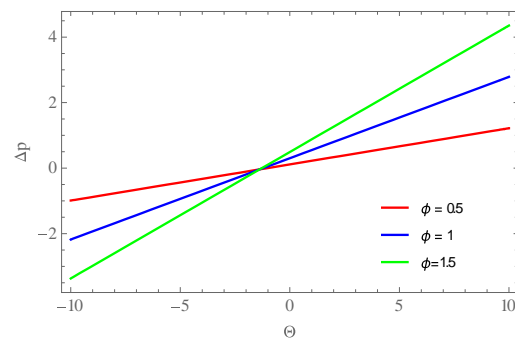


**Figure 16.**The pressure rise for fixed values [ $k = 5, Bn = 5$ ].

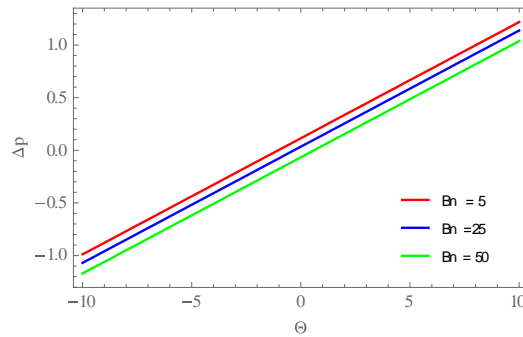


Figure 17. The pressure rise for fixed values [ $k = 5, \phi = 0.5$ ].

#### 4.5 The Stream Lines

Trapping or formation of circular bolus by internally splitting of stream function. The movement of bolus forward through peristaltic wave with the same speed as the wave itself. The bolus or circulation region is symmetric about the center line; it is split into two boluses appearing in the upper and lower halves of the channel for large values of  $k$  where the shape and size of the boluses in the two halves is symmetric. However, for small values of  $k$  the bolus region is not symmetric about the center line  $\eta = 0$ , in fact it is split into two boluses appearing in the upper and lower halves of the channel and the shape and size of the boluses in the two halves is not symmetric. The effect of  $k$  the curvature of the channel on the trapped bolus is shown in **Figure 18**. One can see for small values of  $k$  the bolus decreases in size and number. It is interesting that the size and circulation of the two boluses stops for large values of  $k$ . **Figure 19** deduced that for large values of  $\phi$  and for large values of  $k$  the size and the number of trapped boluses increased where the size and the shape of the bolus is symmetric. **Figure 20** shows that the size and number of the stream lines increases with an increase of  $\phi$  for small values of  $k$  in which the two boluses are not symmetric around the center line  $\eta = 0$ . The impact of flow rate on the stream line in case of large values of  $k$  is shown in **Figure 21**. It shows that for large magnitude of the flow rate the size of the trapping bolus increases. And the impact of flow rate on the stream line in case of small values of  $k$  is shown in **Figure 22**. It shows the size of the trapping bolus increases it is not symmetric around the center line  $\eta = 0$ .

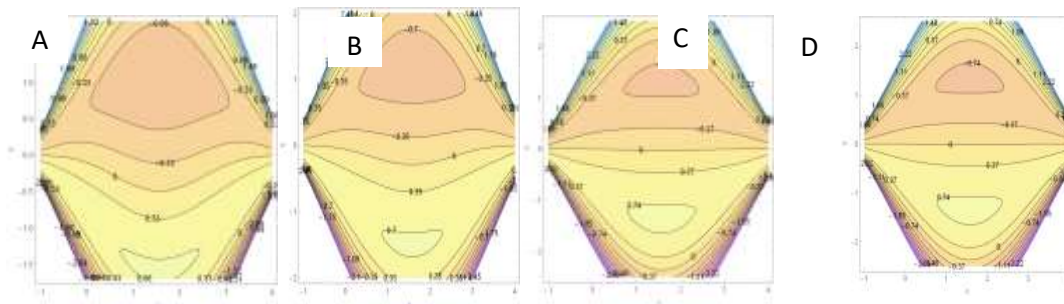


Figure 18. Stream lines for variation of  $k$  and fixed  $\{\phi = 1, k = 5, F = 1\}$  and  $k = 2, k = 5, k = 50, k = 100$ .

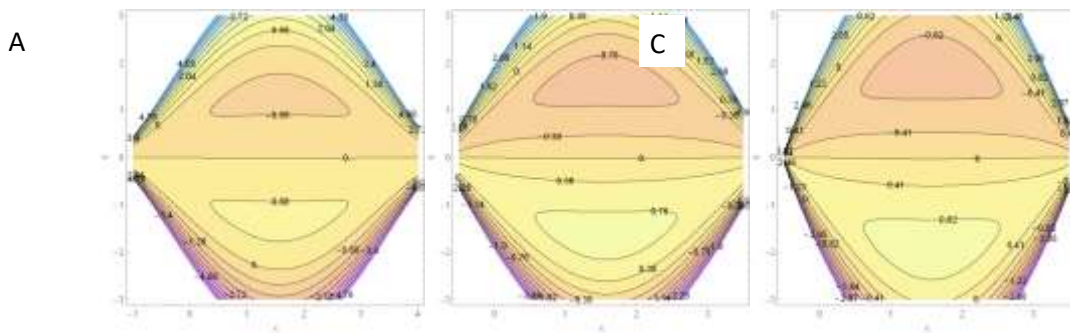


Figure 19. Stream lines for variation of  $\phi$  and fixed  $\{k = 100, F = 1\}$ ,  $\phi = 1, \phi = 1.5, \phi = 2$ .

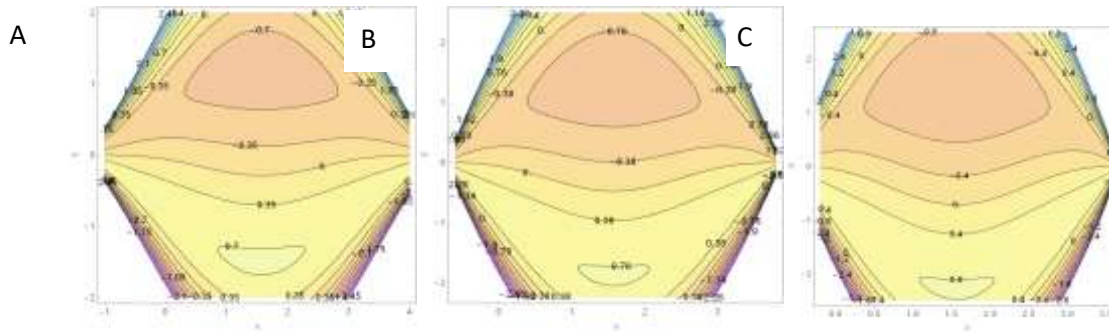


Figure 20. Stream lines for variation of  $\phi$  and fixed  $\{k = 5, F = 1\}$  and  $\phi = 1, \phi = 1.5, \phi = 2$ .

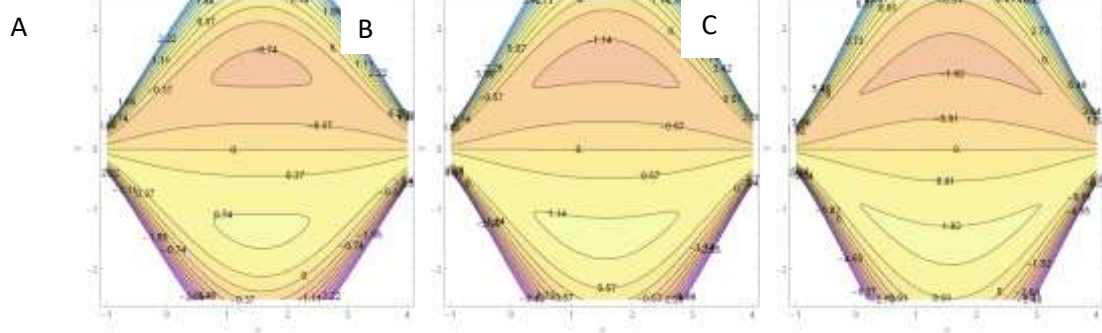


Figure 21. Stream lines for variation of  $F$  and fixed  $\{\phi = 1, k = 100\}$  and  $F = 1, F = 2, F = 3$ .

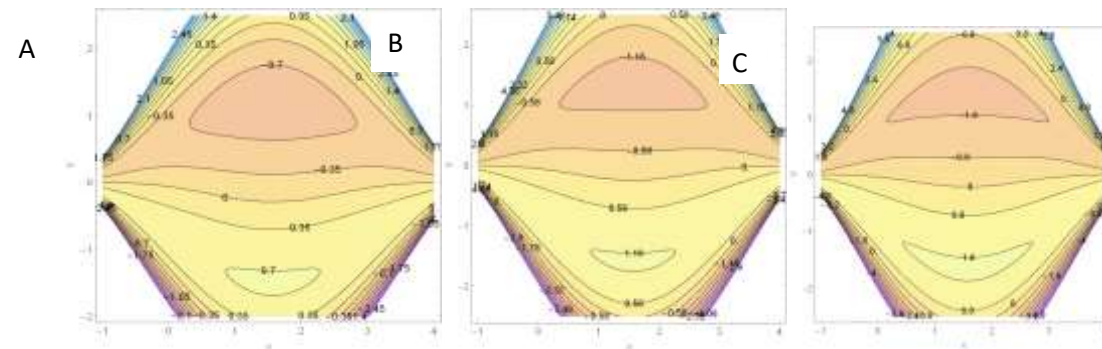


Figure 22. Stream lines for variation of  $F$  and fixed  $\{\phi = 1, k = 5\}$  and  $F = 1, F = 2, F = 3$ .

## 5. Conclusion

In this paper the peristaltic transport of Bingham plastic fluid in a curved channel is examined. Important findings of the analysis have been written as follows:

1. The axial velocity is an increasing function near the walls under the effect of the parameter  $\phi$  and a decreasing function at the central part of the channel. However the situation is reversed for the increase of flow rate.
2. A mixed behavior of local shear stress is noticed due to an increase of  $\phi$ . Shear stress is an increasing function to the increase of  $Bn$  and small values of  $k$ , however the situation is opposite for the increase of  $F$ .
3. The magnitude of pressure gradient decreases with an increase of  $\phi$  and  $Bn$ . However the response is completely reverse with an increase of  $k$ .
4. In the pumping regions, the pumping rate increased in the peristaltic pumping region via increasing of  $\phi$  and  $Bn$ , while the pumping rate increased in the co-pumping region with an increase of  $k$  and  $Bn$ .
5. The size of the trapped bolus increases with an increase of  $\phi$  and  $F$  but the size and shape of the trapped bolus is not symmetric in case of small values of  $k$  and symmetric in case of large values of  $k$ .

## References

1. Adnan, F.A.; Abdualhadi, A.M. Effect of the magnetic field on a peristaltic transport of Bingham plastic fluid. *Jour. of adv. Research and control*.**2018**, *10*, 10, 2007-2024.
2. Ahmad, T.S.; Abdulhadi, A.M. Effect of a magnetic field on peristaltic flow of Jeffery fluid through a porous medium in a tapered asymmetric channel. *Global journal of mathematics*.**2017**, *9*, 2, 6889-6893.
3. Adnan, F.A.; Abdualhadi, A.M. Effect of a magnetic field on a peristaltic transport of Bingham plastic fluid in a symmetrical channel. *Sci. int. (Lhore)*.**2019**, *31*, 1, 29-40
4. Ahmad, T.S.; Abdulhadi, A.M. Peristaltic transport of MHD flow and heat transfer in a tapered asymmetric channel through porous medium: effect of variable viscosity, velocity – non slip and temperature jump. *International journal of Advance scientific and technical research*.**2017**, *7*, 2, 53-69.
5. Ali, N.; Sajid, M.; Abbas, Z. non- Newtonian fluid induced by peristaltic waves in a curved channel. *European journal of mechanic B/fluids*.**2010**, *29*, 387-394.
6. Hayat, T.; Javed, M.; Hendi, A. Peristaltic transport of viscous fluid in curved channel with compliant walls. *International journal of heat and mass transfer*.**2011**, *54*, 1615-1621.
7. Ahmad, T.S.; Abdualhadi, A.M. Effect of radial magnetic field on peristaltic transport of Jeffrey fluid in curved channel with heat and mass transfer. *Journal of physics. conference iop*.**2018**, *1003*, 12053, 1-28.
8. Kalantari, A.; Riasind, A.; Sadeghy, K. Peristaltic flow of Giesekus fluid through curved channels: an approximate solution. *Journal of the society of rhology japan*.**2014**, *42*, 1, 9-17.
9. Norenn, S.; Hayat, T.; Alsaedi, A. Flow of MHD carreau in a curved channel. *Applied Bionics and Bionechanics*.**2013**, *10*, 29-39.
10. Hina, S.; Mustafa, M.; Hayat, T. Peristaltic transport of Johnson - Segalman fluid in a curved channel with slip condition. *Plos one*.**2014**, *9*, 12, 1-25.

11. Sato, H.; Kawai, T.; Fujita, T.; Okabe, M. Two dimensional peristaltic flows in curved channels. Trans. *The Japan soc. Mech. Eng.* **2000**, *66*, 679-688.
12. Tawfiq, L. N. M.; Jabber. A.K. Mathematical Modeling of Groundwater Flow. Global Journal of Engineering science and Researches. **2016**, *3*, *10*, 15-22.